

pubs.acs.org/JPCL Letter

α -MoC Supported Noble Metal Catalysts for Water—Gas Shift Reaction: Single-Atom Promoter or Single-Atom Player

Juan Li, Li Sun, Qiang Wan, Jian Lin, Sen Lin, and Xiaodong Wang*



Cite This: J. Phys. Chem. Lett. 2021, 12, 11415-11421



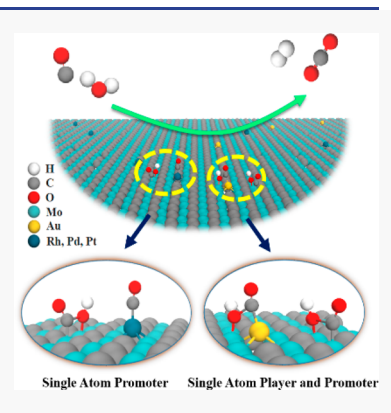
ACCESS I

Metrics & More

Article Recommendations

Supporting Information

ABSTRACT: In this work, we study the water–gas shift (WGS) reaction catalyzed by α -MoC(100) supported typical platinum group metal (PGM) single atoms (Rh₁, Pd₁, and Pt₁) and Au₁ via density functional theory calculations. The adsorption energies of key reaction intermediates and the kinetic barriers of the proposed rate-determining step in the WGS were systematically investigated. It is found that Rh₁, Pd₁, and Pt₁ can serve as single-atom promoters (SAPs) to improve the WGS performance of surface Mo atoms on α -MoC(100). The enhanced activity originates from the fact that SAP modifies the electronic structure of Mo active sites. Comparatively, the Au₁ species not only acts as an SAP but also directly participates in the catalysis as a single-atom player. The additional experiments with single-atom catalyst performance and kinetic studies confirm the theoretical calculation conclusions. This study can provide a basis to further develop efficient WGS catalysts by tuning the activity of the substrate with intercalation of SAPs.



The water–gas shift (WGS) reaction (CO + $H_2O \leftrightarrow CO_2 + H_2$) is a significant process to produce high-purity hydrogen with the decrease of CO impurity that comes from steam reforming of hydrocarbons industrially. This reaction suffers from thermodynamical limit along with decreased CO conversion at increased temperature. Thus, a lower operating temperature is more favored, particularly at <200 °C. Ironand copper-based catalysts have been industrially explored for catalyzing this important process. However, the former encounters the equilibrium-limited problem because of the usual working temperature higher than 350 °C whereas the latter has poorer intrinsic activity at low temperature. Therefore, developing catalysts that have high efficiency to realize WGS reaction at low temperature is urgent but remains a challenge.

Noble metal-based single-atom catalysts (SACs), emerging as a new frontier in heterogeneous catalysis, provide a promising way to catalyze the low-temperature WGS reaction. In the past decade, the advances of catalysts still face inconsistency in the role of single-atom metal species and the underlying substrate. Flytzani-Stephanopoulos et al., proposed that the alkali or OH-stabilized atomically dispersed Au and Pt species played a dominant role in WGS reaction regardless of support on the reducible oxide (e.g., CeO₂ and TiO₂) or the inert substrate (e.g., SiO₂, zeolite, and carbon materials). In comparison, it was found later that the synergistic effect of single-atom metal and support or metal clusters played an important role in the catalysis. For example, we proposed that the dual metal active sites between Ir₁ and Fe of FeO_x support for the WGS reaction proceed via a redox mechanism, which also worked well for Pd₁ or Pt₁ supported on FeO_x catalysts. Ma et al. found the high intrinsic

activity of α -MoC for water dissociation at low-temperature and the cooperation effect of Pt_1 and Pt_n in removing oxygen species on MoC, which can help to increase the stability of MoC-based metal catalysts for a low-temperature WGS reaction.²³

Very recently, we reported a novel Ir_1/α -MoC catalyst that exhibited unprecedented performance in catalyzing the WGS reaction by achieving around 100% CO conversion at 150 °C.²⁴ This is the lowest temperature for the thermodynamic equilibrium conversion that Ir-based catalysts have achieved to date for this reaction. It was found that the Ir_1/α -MoC catalyst had a lower activation energy than the bare MoC catalyst. Nevertheless, the Ir₁ species was not directly involved in the catalysis as a player while serving as a promoter by affecting the electronic properties of the Mo active site. This concept, called as single-atom promoter (SAP), is distinct from the traditional view that the atomically dispersed metal on a support acts as the active site. However, the understanding of the mechanisms and the versatility of the concept of SAP is still incomplete. The relationship between the electronic structures of the SAPmodified active sites over the substrate and the catalytic performance of the WGS reaction needs further clarification.

In this work, we performed investigations on the WGS reaction catalyzed by the α -MoC(100) supported single metal

Received: August 23, 2021 Accepted: October 26, 2021 Published: November 18, 2021





 (M_1) atoms (denoted as M_1/α -MoC(100), $M_1 = Rh_1$, Pd_1 , Pt_1 , and Au₁) from both theoretical and experimental perspectives. The adsorption energies of the key intermediates (CO* and OH*), the electronic structures of the Mo sites modified by M₁, and the kinetic barriers of the proposed rate-determining steps (CO* + OH* \rightarrow COOH*) on M₁/ α -MoC(100) were calculated by density function theory (DFT) calculations, followed by analyzing the electronic effect induced by various SAPs and exploring the corresponding structure-reactivity relationship. This prediction is borne out experimentally with synthesized M_1/α -MoC(100) catalysts, which catalyze the WGS reaction with lower kinetic barrier than that on bare α -MoC(100) catalyst. Similar to the Ir_1/α -MoC case, Rh_1 , Pd_1 , and Pt₁ can also serve as SAPs to enhance the WGS activity of surface Mo atoms on α -MoC because of the significant modification of electronic structure of Mo active sites by the SAPs. In contrast, the Au₁ species not only acts as an SAP but also directly participates in the catalysis as a single-atom player. The in-depth understanding from the combined experimental and theoretical approach is helpful for rational design of new and more effective catalysts by tuning the catalytic activity of substrate with intercalation of an SAP.

Following our previous study on Ir_1/α -MoC,²⁴ we use α -MoC(100) instead of α -MoC(111) because the energy barrier (0.61 eV) for the rate-determining step of WGS on α -MoC(100) is much lower than that (2.25 eV) on α -MoC(111).15 Three typical PGMs (Rh1, Rd1, and Pt1) and the Au₁ single-metal (M₁) atom are chosen to replace a surface Mo or C atom of α -MoC(100). All the computational details are provided in the Supporting Information. The calculated formation energies of M₁ are shown in Table S1. One can see that the substitution of a surface C atom by the M₁ atom is energetically more favorable than the replacing of a surface Mo atom by the M₁ atom because of more negative formation energies. In addition, the doped M₁ has stronger adsorption energy than that for the M_1 adsorption on α -MoC(100) (Table S2). Hence, we focus on only the case of replacing a surface C atom of α -MoC(100) by an M₁ atom, denoted as M_1/α -MoC(100) in the following. The optimized geometries of M_1/α -MoC(100) are shown in Figure S1, in which the introduced M_1 is located above the α -MoC(100) surface and coordinated with four surface Mo atoms, consistent with the former Ir_1/α -MoC(100) model.²⁴

Our DFT studies toward WGS reaction mechanism start from an extensive investigation of the adsorption of CO* and OH*, followed by exploring the kinetics of CO* + OH* \rightarrow COOH*, a mechanism previously reported on Au/ α -MoC and Ir₁/ α -MoC.^{2,24} Two possible reaction routes on different sites are considered on M₁/ α -MoC(100). One is that the reaction takes place on the sole Mo sites (denoted as Mo site mechanism in which M₁ serves as a single-atom promoter, SAP). In this mechanism, the adsorption modes of CO* and OH* are shown in panels a and b of Figure 1, respectively. Another one is that the reaction process is catalyzed with the participation of the single M₁ atom (denoted as M₁ site mechanism in which M₁ is a single-atom player). Under this circumstance, the adsorption patterns of CO* and OH* are displayed in panels c and d of Figure 1, respectively.

For the Mo site mechanism, after introduction of the M_1 , the calculated adsorption energies of CO* and OH* become weaker on Mo atoms in comparison to that on the Mo site of (-1.21 eV for CO* and -3.51 eV for OH*) pristine α -MoC(100) (Figure 2a). In particular, Au_1 has a most

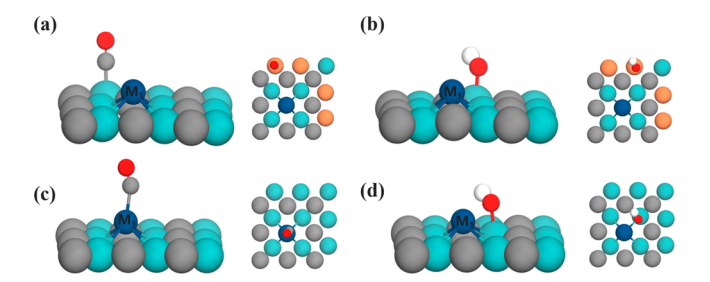


Figure 1. Structural diagrams of the adsorption of CO* (a) and OH* (b) in the Mo site mechanism and the adsorption of CO* (c) and OH* (d) in the M_1 site mechanism on M_1/α -MoC(100), $M_1 = Rh_1$, Pd₁, Pt₁, Au₁. M₁, Mo, C, O, and H atoms are shown in blue, cyan, gray, red, and white, respectively. The Mo atoms involved in the Mo site mechanism are colored orange.

significant impact on the adsorption strength of CO* and OH^* , yielding the binding energies of -0.73 and -3.07 eV, respectively. Furthermore, to obtain a deeper understanding how the M₁ atom affects the adsorption strength of CO* and OH* on Mo sites, electronic structure analysis was carried out. The d-band center (ε_d) is a useful descriptor for evaluating the interaction between transition metals and adsorbates. 25,26 We calculated the projected density of states (PDOSs) of the dorbitals for the active Mo atoms of α -MoC(100) and M_1/α -MoC(100) (Figure S2). As shown in Table S1 and Figure 2b, the $\varepsilon_{\rm d}$ values of surface Mo sites become more negative after intercalating an M_1 atom on α -MoC(100). This is consistent with the change trend for the adsorption energy of CO* and OH*. For example, the ε_d of Mo sites is shifted from -2.24 eV on α -MoC(100) to -2.26 eV on Rh₁/ α -MoC(100). Correspondingly, the adsorption energies of CO* and OH* are reduced from -1.21 and -3.51 eV to -0.91 and -3.25 eV, respectively (Figure 2a). On Au₁/ α -MoC(100), the ε_d of surface Mo sites is significantly shifted to -2.31 eV, inducing much weaker interaction between the CO*/OH* species and the Mo sites (Figure 2a). We calculated the number of delectrons of the four active Mo atoms displayed in Figure 2b by integrating the projected surface d-band density of states up to the Fermi level (called d-band filling).²⁷ It can also be seen from Table S1 and Figure 2b that there is more electron filling into the d-orbitals of the active Mo sites on M_1/α -MoC(100) in comparison to that for pristine α -MoC(100). According to the theory proposed by Nørskov et al., 27-29 the increase of dband filling can lead to the shift of ε_d to lower energy region. The above electronic structure analysis clearly shows a physical picture why the intercalated M₁ atom helps weaken the adsorption strength of CO* and OH* on the surface Mo sites of α -MoC(100).

Subsequently, we investigate the kinetics of CO* + OH* \rightarrow COOH* on M_1/α -MoC(100) following the Mo site mechanism, which was previously identified as the rate-determining step of the WGS process on Ir₁/ α -MoC(100) and other catalysts. Taking Rh₁/ α -MoC(100) as an example, in the initial state, CO* and OH* coadsorb at two adjacent Mo sites. At the transition state, OH* attacks the C atom of CO* with a new forming C-O bond distance of 1.368 Å by overcoming an energy barrier of 0.45 eV. In the final state, the COOH* intermediate is formed. We also calculated the subsequent reaction of COOH* + OH* \rightarrow CO₂* + H₂O* following the Mo site mechanism, and the results show that this reaction step is facile on M_1/α -MoC(100) with a very small barrier (Figure S3), further confirming that CO* + OH*

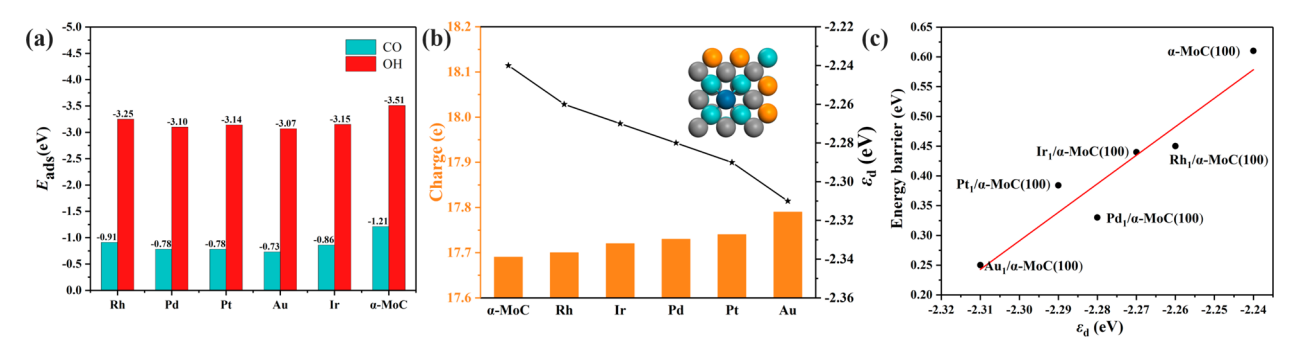


Figure 2. (a) Calculated adsorption energies of CO* and OH* in Mo site mechanism over α -MoC(100) and M_1/α -MoC(100). (b) Relationship between the d-band filling and the d-band center (ε_d) values of the active Mo atoms over α -MoC(100) and M_1/α -MoC(100). (c) Relationship between the ε_d of Mo sites and the energy barrier of CO* + OH* \rightarrow COOH* following Mo site mechanism over α -MoC(100) and M_1/α -MoC(100).

 \rightarrow COOH* is the rate-determining step of the WGS. Interestingly, the barrier of CO* + OH* \rightarrow COOH* on M_1/α -MoC(100) correlates well with the electronic ε_d value of surface Mo sites; namely, the more negative the value of ε_d , the lower the reaction barrier (Figure 2c). The ε_d values vary from -2.31 to -2.26 eV, corresponding to kinetic barriers ranging from 0.25 to 0.45 eV, which is lower than that (0.61 eV) on pristine α-MoC(100). In particular, the surface Mo sites on Au_1/α -MoC(100) has the deepest ε_d , leading to the lowest energy barrier of 0.25 eV. Therefore, the above theoretical calculations predict that the M_1 dopant can be used as a SAP to promote the WGS activity of the surface Mo atoms of α-MoC(100).

To test the theoretical predictions, α -MoC and a series of noble metal single-atom catalysts including α -MoC supported Rh₁, Pd₁, Pt₁, and Au₁ were synthesized through a temperature-programmed carburization method as previously reported.²⁴ SEM was performed to deteremine the morphology, and the M_1/α -MoC (M = Rh, Pd, Pt, Au) catalysts all exhibit porous grains without obvious differences among them (Figure S4). As shown from XRD results (Figure S5), α -MoC is the main crystal phase of the substrate dominated by the (111) and (200) facets, which is not changed after the addition of noble metal species, indicating that the noble metals are highly dispersed on α -MoC. HRTEM results also indicate the dominant exposed crystal planes are α -MoC(111) and (200) on these M_1/α -MoC (M = Rh, Pd, Pt, Au) catalysts (Figure S6). Aberration-corrected high-angle annular dark-field scanning transmission electron microscopy (AC-HAADF-STEM) was performed to visually confirm the metal dispersion on catalysts. As shown in Figures 3 and S7-S10, dispersed Pt, and Au₁ species can be observed on the main facets of α -MoC(111) and α -MoC(200) except for Rh and Pd because of the low contrast of Rh and Pd atoms compared with Mo atoms. EDS mapping was further performed to reflect the dispersion status of Rh and Pd (Figure 3e,f). It can be seen that both Rh and Pd disperse uniformly with no presence of either particles or clusters on α -MoC. Previous studies also proved the facile single-atom form of α -MoC supported metals^{2,12,15,24,33} because α -MoC had abundant surface sites which could provide strong anchoring to the supported metal species.¹⁷ Considering the same preparation method and the similar characters of the series of noble metal catalysts, as well as the strong metal–support interactions of α -MoC supported catalysts, 17 we speculate that the Rh and Pd species also disperse in a single-atom form on α -MoC(111) and α -

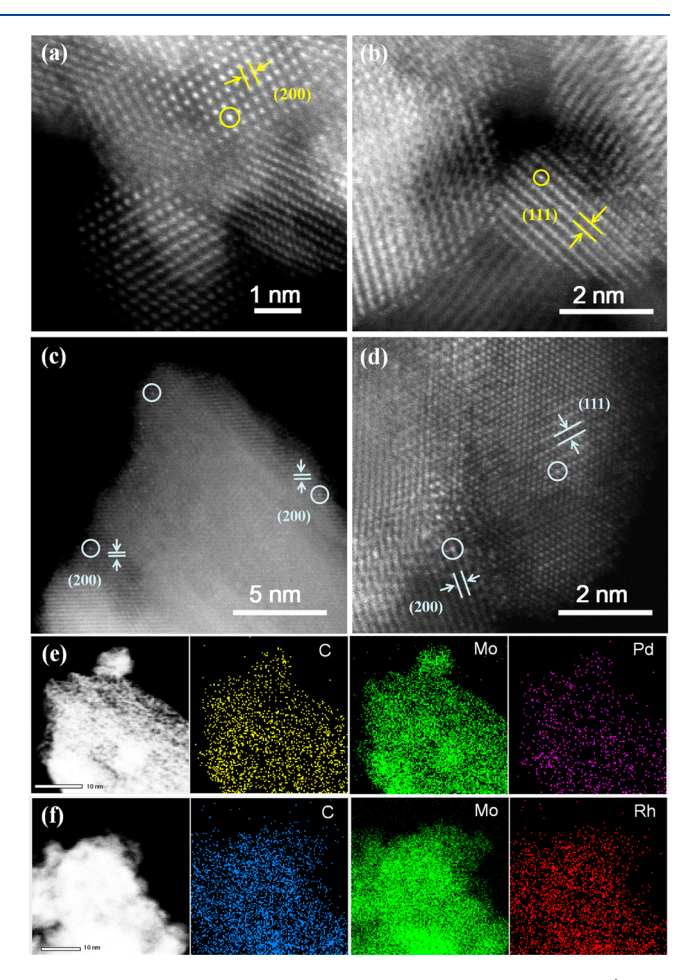


Figure 3. AC-HAADF-STEM images of Au₁/α-MoC catalyst (a and b) and Pt₁/α-MoC catalyst (c and d). The element EDS mappings of Pd₁/α-MoC catalyst (e) and Rh₁/α-MoC catalyst (f). The yellow circles and blue circles indicate Au₁ and Pt₁ single atoms, respectively. The interplanar spacing of α-MoC(200) and α-MoC(111) is 2.14 and 2.47 Å, respectively.

MoC(200). However, the current results in this work do not prove which plane the single atom is more loaded on, and more evidence is needed to clarify this issue in the future.

Performance tests were then carried out on the above synthesized $M_1/\alpha\text{-MoC}$ catalysts. As shown in Figure 4a, the activities of $M_1/\alpha\text{-MoC}$ catalysts were consistently higher than the bare $\alpha\text{-MoC}$ at all reaction temperatures and approached the thermodynamic limit before 175 °C for the low-

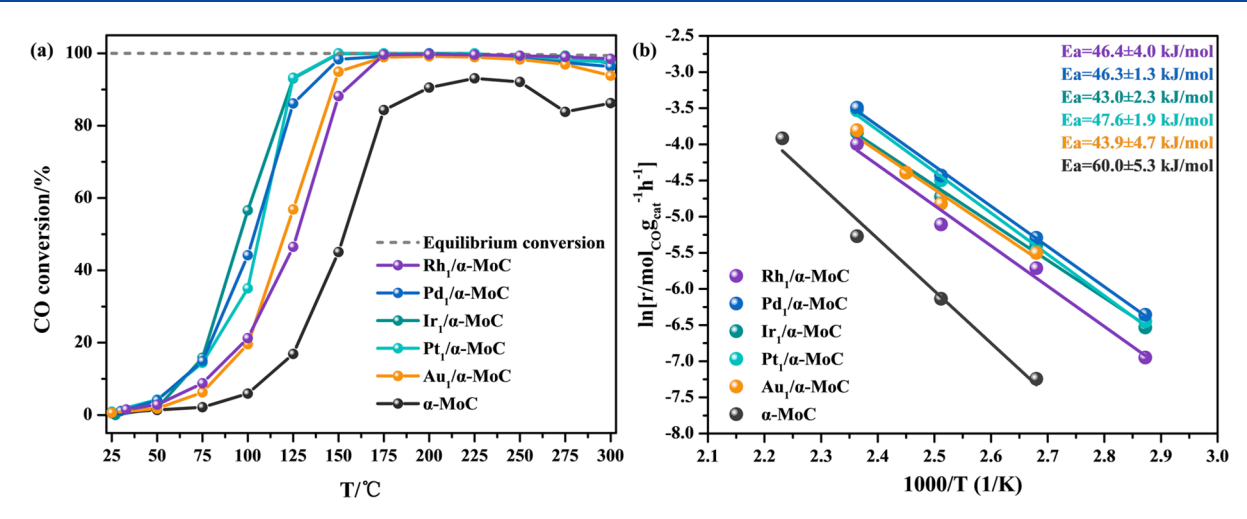


Figure 4. CO conversion as a function of reaction temperature (a) and Arrhenius plots (b) for M_1/α -MoC (M_1 = Rh₁, Pd₁, Pt₁, Ir₁ and Au₁) and α-MoC catalysts for WGS reaction. The data of Ir₁/α-MoC is from ref 24.

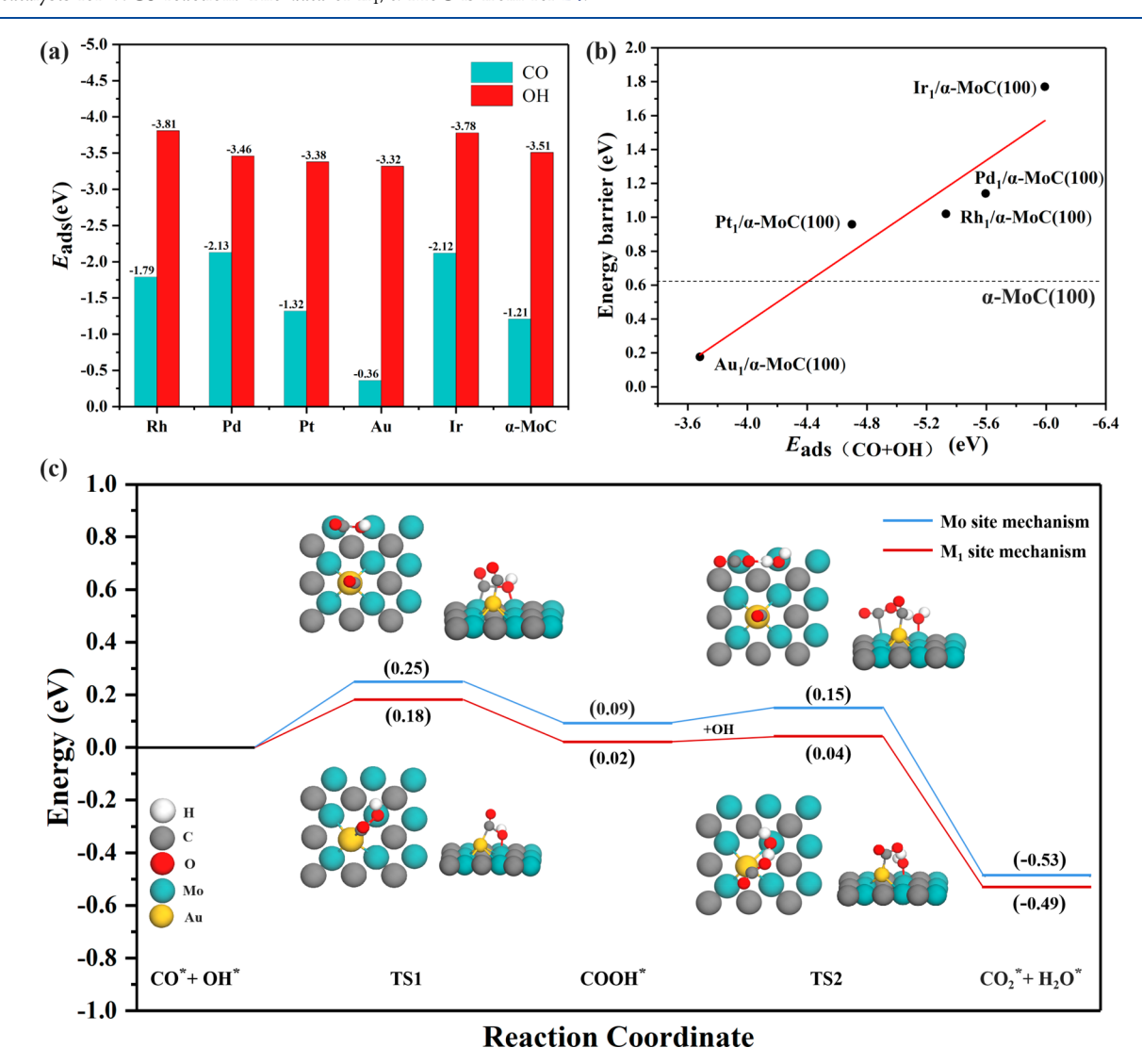


Figure 5. (a) Calculated adsorption energies of CO* and OH* over M_1/α -MoC(100) in M_1 site mechanism compared with those on the Mo sites of α -MoC(100). (b) Relationship between the activation energy (E_a) of CO* + OH* \rightarrow COOH* and the sum of CO* and OH* adsorption energies on α -MoC(100) and M_1/α -MoC(100). (c) Calculated energy pathways for WGS reaction following Mo site and M_1 site mechanisms on Au_1/α -MoC(100) with side and top views for the structures of the transition states (TSs).

temperature WGS reaction. In detail, Pd_1/α -MoC, Ir_1/α -MoC, and Pt_1/α -MoC catalysts exhibit almost the same CO conversion profiles while Rh_1/α -MoC presents less active performance. It should be noted that Au_1/α -MoC exhibits lower CO conversions because a lower loading amount of Au is used to keep it in a single-atom catalyst form as Au is apt to sinter with a low Tammann temperature. 34,35 Then the specific rates were evaluated in the kinetic regime by keeping the CO conversion below 15% to make an intrinsic comparison. The reaction rates are reported in the form of Arrhenius plots in Figure 4b with the apparent activation energy values labeled in the diagram. The overall reaction rates were measured based on the amount of catalyst to focus on the substrate contribution. It can be seen that M_1/α -MoC ($M_1 = Rh_1$), Pd₁, Ir₁, Pt₁, and Au₁) catalysts exhibit similar reaction rates that are much higher than that of α -MoC. Table S3 also shows the similar promotion effects of different α -MoC supported catalysts with mass specific rate at the same order of magnitude, while this performance is much higher than those of other support-based catalysts previously reported. The calculated values for the apparent activation energy (E_a) of the M_1/α -MoC are all lower than that on α -MoC (\sim 60 kJ/mol). We can find that the difference of these E_a values among M_1/α -MoC is relatively smaller than that for the calculated energy barriers of rate-determining step (Figure 2c), which might be attributed to the catalyst containing (111) and (100) facets in the experiment while only the (100) model is used in DFT calculations, and the coverage effect which was not taken into account in DFT calculations. Nevertheless, these results support the conclusion that the M₁ dopant can modify the α -MoC surface by reducing the energy barrier and thus increase the catalytic activity of the WGS reaction. The AC-HAADF-STEM and EDS experiments were also performed on the used catalysts, which show that the metal species are still in the single-metal form without sintering after reaction (Figure S11).

To answer the possibility whether M₁ can act as an active site, we then theoretically examine the WGS reaction proceeding via an M_1 site mechanism on M_1/α -MoC(100), in which the CO molecule adsorbed on the M₁ site can directly react with the OH* species located on an adjacent Mo sites. As shown in Figure 5a, under this circumstance, the adsorption energies of OH^* range from -3.32 to -3.81 eV, comparable to that (-3.51 eV) on the pristine α -MoC(100), while the adsorption energies of CO^* on M_1 ($M_1 = Rh_1$, Pd_1 , and Pt_1) are larger than that (-1.21 eV) on the Mo sites of bare α -MoC(100). Surprisingly, the binding energy of CO* on Au₁ supported by α -MoC(100) is only -0.36 eV, suggesting that $CO^* + OH^* \rightarrow COOH^*$ might take place via the M₁ site mechanism based on the Brønsted-Evans-Polanyi (BEP) relationship.³⁶ Interestingly, the calculated energy barrier of this reaction on M_1/α -MoC(100) following the M_1 site mechanism exhibits a good linear relationship with the sum of adsorption energies of CO* and OH* (Figure 5b). The comparison of reaction barriers of CO* + OH* → COOH* via the M₁ site mechanism and Mo site mechanism displayed in Figures 2c and 5b precludes the intercalated Rh₁, Pd₁, Pt₁, and Ir_1 species as active sites on α -MoC(100) because of the extremely high energy barriers.

In contrast, it should be noted that the calculated kinetic barrier for CO* + OH* \rightarrow COOH* via the M₁ site mechanism is significantly reduced to 0.18 eV on Au₁/ α -MoC(100), much less than that (0.61 eV) on the α -

MoC(100) surface but very close to that (0.25 eV) via the Mo site mechanism (Figure 5b,c). This is because the weak interaction between the adsorbed CO* species and the supported Au₁ suppresses the poison of Au₁ site by CO molecule. Moreover, regardless of the Mo site mechanism or M₁ site mechanism, the COOH* intermediate can facilely react with an adjacent OH* to produce CO₂* and H₂O* by overcoming a minor barrier. The above DFT results regarding the mechanism studies reveal that the α -MoC(100) supported single Au₁ atom not only acts as a single-atom promoter but also serves as a single-atom player in the catalysis of the WGS reaction

To obtain a deeper understanding of the host-guest role between MoC substrate and Au₁ single atom in the WGS reaction, we measured the reaction orders of CO and H₂O on Au_1/α -MoC with Ir_1/α -MoC catalyst as a comparison, which present the lowest and highest value of energy barrier through the M_1 site mechanism (Figure 5b). As shown in Figure S12a, the reaction order of CO approaches zero over ${\rm Ir_1}/\alpha{\rm -MoC}$. This suggests the independence of WGS reaction rates on CO pressure over Ir_1/α -MoC, probably because of the facile CO adsorption and the almost complete coverage on active sites, 30,37 which can originate from the high adsorption strength of CO* on the Ir₁ site (-2.12 eV, Figure 5a) and also the moderate strength (-0.86 eV, Figure 2a) on the Mo site modified by Ir₁. In contrast, the CO order is much higher with ~ 0.38 over Au₁/ α -MoC, indicating more dependence of reaction rates on the adsorption of CO*, which can be attributed by the much weaker adsorption strength whether on the Au_1 site (-0.36 eV, Figure 5a) or on the promoted Mo site (-0.73 eV, Figure 2a). Meanwhile, the reaction orders of H₂O over Ir_1/α -MoC and Au_1/α -MoC catalysts are almost zero (Figure S12b), on account of the facile activation and complete saturation of H_2O on the substrate of α -MoC.² These observations correlate well with the DFT results on $\mathrm{Au_1}/\alpha$ -MoC where the M₁ site mechanism and the Mo site mechanism are both feasible, whereas on the α -MoC supported PGM single-atom catalysts the reaction proceeds dominantly through the Mo site mechanism.

In summary, we studied the adsorption behavior of CO* and OH*, two key intermediates in the WGS reaction, and the key step (CO* + OH* \rightarrow COOH*) on α -MoC(100) supported Rh₁, Pd₁, Pt₁, and Au₁ catalysts using DFT calculations. The results show that the single metal atom makes the adsorption energies of CO* and OH* become weaker on the surface Mo atoms than on Mo site of bare α -MoC(100). The reason can be well explained by the electronic structure analysis; that is, extra electron filling into the d orbitals of Mo active sites led to the shift of the d-band center to the lower energy region after intercalating an M_1 atom on α -MoC(100). Kinetically, the barriers of $CO^* + OH^* \rightarrow$ COOH* taking place on the Mo sites of M_1/α -MoC(100) range from 0.25 to 0.45 eV, lower than that (0.61 eV) on pristine α -MoC(100). In this mechanism, M_1 serves as a single-atom promoter to enhance the WGS activity of Mo sites on α -MoC(100). On the other hand, CO* + OH* \rightarrow COOH* directly occurring on the Rh₁, Pt₁, and Pd₁ sites requires high barriers ranging from 0.96 to 1.14 eV owing to the relatively strong adsorption of CO* on the M₁ site. In comparison, this reaction step can proceed on the Au₁ site with a much lower barrier of 0.18 eV due to weak interaction between CO* and Au₁, which suggests that the Au₁ species can not only act as a single-atom promoter but also serve as a

single-atom player in the catalysis. The experimental studies further substantiate the theoretical calculations that the intercalation of M_1 dopants greatly enhances the WGS activity of α -MoC while the α -MoC supported Au_1 species has dual role in the catalysis. These explorations will help to better understand the relationship between the electronic structure and catalytic behavior on a microscopic scale, thereby benefitting the rational design of catalysts for high-efficiency WGS reaction.

ASSOCIATED CONTENT

5 Supporting Information

The Supporting Information is available free of charge at https://pubs.acs.org/doi/10.1021/acs.jpclett.1c02762.

Additional experimental and theoretical results (PDF)

AUTHOR INFORMATION

Corresponding Authors

Jian Lin — CAS Key Laboratory of Science and Technology on Applied Catalysis, Dalian Institute of Chemical Physics, Chinese Academy of Sciences, Dalian 116023, P.R. China; orcid.org/0000-0002-1084-7446; Email: jianlin@dicp.ac.cn

Sen Lin — State Key Laboratory of Photocatalysis on Energy and Environment, College of Chemistry, Fuzhou University, Fuzhou 350002, P.R. China; orcid.org/0000-0002-2288-5415; Email: slin@fzu.edu.cn

Xiaodong Wang — CAS Key Laboratory of Science and Technology on Applied Catalysis, Dalian Institute of Chemical Physics, Chinese Academy of Sciences, Dalian 116023, P.R. China; orcid.org/0000-0002-8705-1278; Email: xdwang@dicp.ac.cn

Authors

Juan Li – State Key Laboratory of Photocatalysis on Energy and Environment, College of Chemistry, Fuzhou University, Fuzhou 350002, P.R. China

Li Sun — CAS Key Laboratory of Science and Technology on Applied Catalysis, Dalian Institute of Chemical Physics, Chinese Academy of Sciences, Dalian 116023, P.R. China; University of Chinese Academy of Sciences, Beijing 100049, P.R. China

Qiang Wan — State Key Laboratory of Photocatalysis on Energy and Environment, College of Chemistry, Fuzhou University, Fuzhou 350002, P.R. China; orcid.org/0000-0001-7711-6747

Complete contact information is available at: https://pubs.acs.org/10.1021/acs.jpclett.1c02762

Author Contributions

^{II}J. Li and L. Sun contributed equally.

Notes

The authors declare no competing financial interest.

■ ACKNOWLEDGMENTS

This paper is dedicated to the celebration of the 10th Anniversary of the Founding of the Youth Innovation Promotion Association of the Chinese Academy of Sciences. We thank the National Natural Science Foundation of China (21973013, 21673040, 22022814, 21878283, and 21962007); the National Natural Science Foundation of Fujian Province, China (2020J02025); the "Chuying Program" for the Top

Young Talents of Fujian Province; and the Youth Innovation Promotion Association CAS (2017223)

REFERENCES

- (1) LeValley, T. L.; Richard, A. R.; Fan, M. The progress in water gas shift and steam reforming hydrogen production technologies A review. *Int. J. Hydrogen Energy* **2014**, 39 (30), 16983–17000.
- (2) Yao, S.; Zhang, X.; Zhou, W.; Gao, R.; Xu, W.; Ye, Y.; Lin, L.; Shi, C.; Rodriguez, J. A.; Ma, D.; et al. Atomic-layered Au clusters on α -MoC as catalysts for the low-temperature water-gas shift reaction. *Science* **2017**, 357 (6349), 389–393.
- (3) Rodriguez, J. A.; Graciani, J.; Evans, J.; Park, J. B.; Yang, F.; Stacchiola, D.; Senanayake, S. D.; Ma, S.; Perez, M.; Liu, P.; et al. Water-gas shift reaction on a highly active inverse $CeO_x/Cu(111)$ catalyst: unique role of ceria nanoparticles. *Angew. Chem., Int. Ed.* **2009**, 48 (43), 8047–8050.
- (4) Ratnasamy, C.; Wagner, J. P. Water gas shift catalysis. *Catal. Rev.: Sci. Eng.* **2009**, 51 (3), 325-440.
- (5) Lustemberg, P. G.; Feria, L.; Ganduglia-Pirovano, M. V. Single Ni sites supported on CeO₂(111) reveal cooperative effects in the water—gas shift reaction. *J. Phys. Chem. C* **2019**, *123* (13), 7749—7757.
- (6) Rodriguez, J. A.; Remesal, E. R.; Ramírez, P. J.; Orozco, I.; Liu, Z.; Graciani, J.; Senanayake, S. D.; Sanz, J. F. Water—gas shift reaction on K/Cu(111) and $Cu/K/TiO_2(110)$ surfaces: alkali promotion of water dissociation and production of H_2 . ACS Catal. **2019**, 9 (12), 10751-10760.
- (7) Zugic, B.; Zhang, S.; Bell, D. C.; Tao, F.; Flytzani-Stephanopoulos, M. Probing the low-temperature water—gas shift activity of alkali-promoted platinum catalysts stabilized on carbon supports. *J. Am. Chem. Soc.* **2014**, *136* (8), 3238—3245.
- (8) Alijani, A.; Irankhah, A. Medium-temperature shift catalysts for hydrogen purification in a single-stage reactor. *Chem. Eng. Technol.* **2013**, 36 (2), 209–219.
- (9) Wang, G.-C.; Nakamura, J. Structure sensitivity for forward and reverse water-gas shift reactions on copper surfaces: A DFT study. *J. Phys. Chem. Lett.* **2010**, *1* (20), 3053–3057.
- (10) Senanayake, S. D.; Sadowski, J. T.; Evans, J.; Kundu, S.; Agnoli, S.; Yang, F.; Stacchiola, D.; Flege, J. I.; Hrbek, J.; Rodriguez, J. A. Nanopattering in CeO_x/Cu(111): A new type of surface reconstruction and enhancement of catalytic activity. *J. Phys. Chem. Lett.* **2012**, 3 (7), 839–843.
- (11) Li, Q.; Ma, Z.; Sa, R.; Adidharma, H.; Gasem, K. A. M.; Russell, A. G.; Fan, M.; Wu, K. Computation-predicted, stable, and inexpensive single-atom nanocatalyst Pt@Mo₂C an important advanced material for H₂ production. *J. Mater. Chem. A* **2017**, 5 (28), 14658–14672.
- (12) Li, S.; Cao, R.; Xu, M.; Deng, Y.; Lin, L.; Yao, S.; Liang, X.; Liu, J.-X.; Zhou, W.; Ma, D. Atomically dispersed Ir/α -MoC catalyst with high metal loading and thermal stability for water-promoted hydrogenation reaction. *Natl. Sci. Rev.* **2021**, nwab026 DOI: 10.1093/nsr/nwab026.
- (13) Flytzani-Stephanopoulos, M. Gold atoms stabilized on various supports catalyze the water—gas shift reaction. *Acc. Chem. Res.* **2014**, 47 (3), 783—792.
- (14) Ding, K.; Gulec, A.; Johnson, A. M.; Schweitzer, N. M.; Stucky, G. D.; Marks, L. D.; Stair, P. C. Identification of active sites in CO oxidation and water-gas shift over supported Pt catalysts. *Science* **2015**, 350 (6257), 189–192.
- (15) Lin, L.; Zhou, W.; Gao, R.; Yao, S.; Zhang, X.; Xu, W.; Zheng, S.; Jiang, Z.; Yu, Q.; Ma, D.; et al. Low-temperature hydrogen production from water and methanol using Pt/α -MoC catalysts. *Nature* **2017**, *544* (7648), 80–83.
- (16) Farnesi Camellone, M.; Marx, D. On the impact of solvation on a Au/TiO_2 nanocatalyst in contact with water. *J. Phys. Chem. Lett.* **2013**, *4* (3), 514–518.
- (17) Dong, J.; Fu, Q.; Jiang, Z.; Mei, B.; Bao, X. Carbide-supported Au catalysts for water-gas shift reactions: A new territory for the

- strong metal-support interaction effect. J. Am. Chem. Soc. 2018, 140 (42), 13808-13816.
- (18) Yang, M.; Flytzani-Stephanopoulos, M. Design of single-atom metal catalysts on various supports for the low-temperature water-gas shift reaction. *Catal. Today* **2017**, 298, 216–225.
- (19) Zhai, Y.; Pierre, D.; Si, R.; Deng, W.; Ferrin, P.; Nilekar, A. U.; Peng, G.; Herron, J. A.; Mavrikakis, M.; Flytzani-Stephanopoulos, M.; et al. Alkali-stabilized Pt-OH_x species catalyze low-temperature watergas shift reactions reactions. *Science* **2010**, 329 (5999), 1633–1636.
- (20) Liang, J. X.; Lin, J.; Liu, J.; Wang, X.; Zhang, T.; Li, J. Dual metal active sites in an ${\rm Ir_1}$ /FeO_x single-atom catalyst: A redox mechanism for the water-gas shift reaction. *Angew. Chem., Int. Ed.* **2020**, *59* (31), 12868–12875.
- (21) Chen, Y.; Lin, J.; Li, L.; Qiao, B.; Liu, J.; Su, Y.; Wang, X. Identifying size effects of Pt as single atoms and nanoparticles supported on ${\rm FeO_x}$ for the water-gas shift reaction. *ACS Catal.* **2018**, 8 (2), 859–868.
- (22) Sun, X.; Lin, J.; Zhou, Y.; Li, L.; Su, Y.; Wang, X.; Zhang, T. FeO_x supported single-atom Pd bifunctional catalyst for water gas shift reaction. AIChE J. **2017**, 63 (9), 4022–4031.
- (23) Zhang, X.; Zhang, M.; Deng, Y.; Xu, M.; Artiglia, L.; Wen, W.; Flytzani-Stephanopoulos, M.; Shi, C.; Zhou, W.; Ma, D.; et al. A stable low-temperature H_2 -production catalyst by crowding Pt on α -MoC. *Nature* **2021**, 589 (7842), 396–401.
- (24) Sun, L.; Xu, J.; Liu, X.; Qiao, B.; Li, L.; Lin, J.; Lin, S.; Wang, X.; Guo, H.; Zhang, T.; et al. High-efficiency water gas shift reaction catalysis on α -MoC promoted by single-atom Ir species. *ACS Catal.* **2021**, *11* (10), 5942–5950.
- (25) Hammer, B.; Nørskov, J. K. Theoretical surface science and catalysis calculations and concepts. *Adv. Catal.* **2000**, *45*, 71–129. (26) Mavrikakis, M.; Hammer, B.; Nørskov, J. K. Effect of strain on the reactivity of metal surfaces. *Phys. Rev. Lett.* **1998**, *81* (13), 2819–
- (27) Nørskov, J. K.; Abild-Pedersen, F.; Studt, F.; Bligaard, T. Density functional theory in surface chemistry and catalysis. *Proc. Natl. Acad. Sci. U. S. A.* **2011**, *108* (3), 937–943.

2822.

- (28) Kitchin, J. R.; Nørskov, J. K.; Barteau, M. A.; Chen, J. G. Modification of the surface electronic and chemical properties of Pt(111) by subsurface 3d transition metals. *J. Chem. Phys.* **2004**, *120* (21), 10240–10246.
- (29) Kitchin, J. R.; Nørskov, J. K.; Barteau, M. A.; Chen, J. G. Role of strain and ligand effects in the modification of the electronic and chemical properties of bimetallic surfaces. *Phys. Rev. Lett.* **2004**, *93* (15), 156801.
- (30) Nelson, N. C.; Nguyen, M.-T.; Glezakou, V.-A.; Rousseau, R.; Szanyi, J. Carboxyl intermediate formation via an in situ-generated metastable active site during water-gas shift catalysis. *Nat. Catal.* **2019**, 2 (10), 916–924.
- (31) Gokhale, A. A.; Dumesic, J. A.; Mavrikakis, M. On the mechanism of low-temperature water gas shift reaction on copper. *J. Am. Chem. Soc.* **2008**, *130* (4), 1402–1414.
- (32) Wang, J. G.; Hammer, B. Theoretical study of H₂O dissociation and CO oxidation on Pt₂Mo(111). *J. Catal.* **2006**, 243 (1), 192–198.
- (33) Ma, Y.; Ren, Y.; Zhou, Y.; Liu, W.; Baaziz, W.; Ersen, O.; Pham-Huu, C.; Greiner, M.; Chu, W.; Wang, A.; et al. High-density and thermally stable palladium single-atom catalysts for chemoselective hydrogenations. *Angew. Chem., Int. Ed.* **2020**, *59* (48), 21613–21619.
- (34) Haruta, M.; Yamada, N.; Kobayashi, T.; Iijima, S. Gold catalysts prepared by coprecipitation for low-temperature oxidation of hydrogen and of carbon monoxide. *J. Catal.* **1989**, *115* (2), 301–309.
- (35) Veith, G. M.; Lupini, A. R.; Rashkeev, S.; Pennycook, S. J.; Mullins, D. R.; Schwartz, V.; Bridges, C. A.; Dudney, N. J. Thermal stability and catalytic activity of gold nanoparticles supported on silica. *J. Catal.* **2009**, 262 (1), 92–101.
- (36) Ferrin, P.; Simonetti, D.; Kandoi, S.; Kunkes, E.; Dumesic, J. A.; Nørskov, J. K.; Mavrikakis, M. Modeling ethanol decomposition on transition metals: A combined application of scaling and brønstedevans-polanyi relations. *J. Am. Chem. Soc.* **2009**, *131* (16), 5809–5815.

(37) Azzam, K. G.; Babich, I. V.; Seshan, K.; Lefferts, L. Role of Re in Pt-Re/TiO₂ catalyst for water gas shift reaction: A mechanistic and kinetic study. *Appl. Catal., B* **2008**, *80* (1), 129–140.